Effect of Starting Particle Size on the Evolution of Hydroxyapatite from Cattle Bone Waste for Biomedical Applications

C. S. Obayi[1, 2, *], E. C. Ugwu[1], H. A. Obe[1], P. C. Ekedebe[1], M. O. Egbuhuzor[1, 2], P. O. Offor[1, 2] and P. S. Nnamchi[2]

[1]*Department of Metallurgical and Materials Engineering, University of Nigeria, Nsukka, Enugu State, Nigeria*
[2]*Department of Biomedical Engineering, University of Nigeria*
*Corresponding author: camillus.obayi@unn.edu.ng

Received 10/08/2025; accepted 20/02/2026
https://doi.org/10.4152/pea.2027450518

Abstract
This work sought to establish whether starting particle size (SPS) is an important parameter on the properties of hydroxyapatite (HAP) extracted from cattle bone (CB) waste material by heat treatment, for biomedical applications, such as temperature and holding time. CB was processed to obtain micron-sized particles of 50, 150, 250 and 350 μm. The powders were heated to a constant temperature and holding time of 900 °C and 3 h, respectively, to enable their transformation into HAP. Evolved HAP was characterized using X-ray diffraction (XRD), scanning electron microscopy (SEM), energy dispersive X-ray spectroscopy (EDX) and Fourier transform infrared spectroscopy (FTIR). Results indicated that physico-chemical properties were very sensitive to SPS of CB. XRD results revealed that crystallite size and degree of crystallinity of evolved HAP increased with greater SPS. Based on EDX results, concentration of essential elements of Ca, P, O and C in HAP also varied according to SPS increasing from 36.0 to 50.5 wt. % for Ca, decreasing from 13.7 to 9.9 wt. % for P, 36.2 to 29.6 wt. % for O and 12.6 to 9.3 wt. % for C. FTIR spectra indicated that concentration of functional groups is sensitive to SPS, with amounts of OH^- and PO_4^{3-} increasing, while CO_3^{2-} decreased with an increase in SPS. Thus, SPS is an important parameter in evolution of HAP from CB waste via calcination process.

Keywords: biomedical; CB waste; evolution; HAP; SPS.

Introduction•

Hydroxyapatite (HAP) is a very important bio-ceramic that is extensively used for bone substitution and dental reconstruction. Its popularity in the above applications stems from its similarity to major mineral constituents of human bone and teeth, and its ease of forming chemical bonds with hard bone tissues [1]. Besides being used in

•The abbreviation list is in page 624.

orthopaedics and dentistry, HAP is also employed in drug delivery and wound dressing due to its biocompatibility and bioactivity. HAP is also applied in nonmedical fields such as biosensing and water purification [2].

Due to the importance of HAP in biomedical applications, its production has been done both synthetically and naturally from animal bones. Its extraction from organic sources is preferred because natural HAP has essential trace elements found in bones such as Na, Mag, Al, Fe, and minerals like CO_3^{2-} which are beneficial for bone growth and supporting biological functions [3-5]. Furthermore, extraction of HAP from natural sources is less expensive, as raw materials are readily available. Naturally, HAP is extracted from animal waste sources such as mammalian and fish bones [6-9], and shells [10, 11], and synthetically from chemical species such as $Ca_2P_2O_4$, Na_2HPO and K_2HPO.

Among several techniques used in preparing HAP from natural sources, such as mechanochemical synthesis [12, 13], precipitation methods [14], microwave processing [15], solid-state [16] and wet chemical procedures [17], calcination and sintering method is popular [18-25]. Calcination involves heating natural bone powders to high temperatures for certain time durations to enable elimination of organic matter and evolution of HAP. Temperature and holding time are important parameters that impact evolution of HAP from natural bone powders and its properties [20]. Some of the properties of HAP affected by processing methods include evolved crystallite size, crystallinity, Ca/P ratios, composition and surface area.

Currently, controlling the grain size of evolved HAP during processing is very important because its size determines its effectiveness for specific applications [7, 26]. Evolved crystallite size and crystallinity of HAP have been found to affect its drug loading capacity, drug release rate [27] and bio-resorption [28]. Besides improving biological activities of HAP, reduction of grain size from micro to nano level significantly improves bioactivity, biocompatibility and mechanical properties, such as toughness and hardness [29, 30]. Processing methods are now being maneuvered to obtain HAP with very small grain sizes for the obvious reason of harnessing the advantage of small-grained materials.

This work sought to understand the effect of SPS on properties of HAP extracted from cattle bone (CB) waste. To the best of the authors' knowledge, there is no work that has specifically considered the influence of SPS of CB waste material on evolved crystallite size, Ca/P ratio, crystallography, compositional and morphological properties of synthesized HAP using calcination method. The outcome of this work contributes to adding to important parameters that influence evolution of HAP from animal bone waste via calcination or heating treatment.

Furthermore, the successful outcome of this research promotes utilization of CB waste for production of HAP, thereby repurposing waste materials for environmental sustainability and contribution to the circular economy. Successful synthesis of high-quality HAP from CB waste reduces reliance on synthetic or chemically derived HAP,

lowering production costs and minimizing environmental impact [31]. This is particularly significant as demand for bio-based materials in medical and dental fields continues to rise.

Materials and methods

Materials

Materials used for preparation of HAP were: CB femur, which was sourced from an abattoir at Ogige market, Nsukka, Nigeria; distilled water for washing and cleaning bones; and acetone for de-fatting cleaned bones. Other materials were: pestle and mortar for crushing CB into small pieces; grinding machine for pulverizing bones into smaller particles; a sieve for separating particles into four particle sizes (50, 150, 250 and 300 μm); and a muffle furnace for heat treatment of the bone powder.

Methods

Preparation and calcination of CB particles

Sourced CB waste was boiled in water for 1 h, to enable easy defatting and removal of impurities. This was followed by washing and rinsing bones several times in distilled water, in order to remove meat, tendons, bone marrow and soft tissues. Washed CB were soaked in acetone for 2 h, and washed again with distilled water several times to remove invisible fat. The bones were then sun-dried for 4 weeks to evaporate adsorbed moisture, and further dried in an oven at 2000 °C, for 1 h, to reduce absorbed water and some organic matter. Dried cow bone was crushed into smaller pieces in a crusher, followed by pulverization using a grinding machine and sieving to obtain particle sizes, hereafter referred to as starting particle sizes (SPS) of CB material.

15 g each of sieved CB powder were measured out for calcination. In order to reduce oxidation, measured powder was placed separately in a small ceramic container with a lid sealed with clay material. Sealed ceramic containers were placed in a muffle furnace, and heated at a rate of 10 °C per min, to a constant temperature of 900 ºC, and a constant holding time of 3 h. Calcined samples were then cooled slowly to room temperature, followed by an evaluation of their physico-chemical properties.

Crystallographic, compositional and morphological characterization

Crystallographic composition of uncalcined and calcined bone particles was determined using a Drywell Diffractometer (DW-XRD-2700A), China, operated at 45 kV and 40 mA, with a Cu-Kα (λ = 1.54 Å) in the range of 2θ = 10°–70°, at a step size of 0.02°. Degree of crystallinity (X_c) was calculated using Eq. (1) as in [32], while crystallite size (D) in nanometres was obtained employing Scherrer's Eq. (2).

$$X_c(\%) = 1 - \frac{I_{112/300}}{I_{300}} \quad (1)$$

where $I_{112/300}$ is intensity of valley (hollow part) between peaks (112) and I_{300} is intensity of the peak (300).

$$D = \frac{K\lambda}{\beta cos\theta} \quad (2)$$

where K is constant for spherical crystallite, K is 0.89; β is full width at half maximum of the peak (FWHM) in radians, λ is diffraction wavelength (0.154059 nm or 1.54059) and θ is diffraction angle.

Functional groups present in uncalcined and calcined bone samples were confirmed using a Nicolet spectrometer (Magna-IR 560), USA, in the range from 4000 to 400 cm^{-1}. Morphology of uncalcined and calcined bone samples was examined using SEM (VEGA3 TESCAN), Czech Republic, and equipped EDX, which enabled determination of elemental composition of the samples.

Results and discussion

Crystallographic analysis of uncalcined and calcined CB samples

XRD patterns of the uncalcined sample and samples calcined at a constant temperature of 900 °C and a holding time of 3 h, compared to standard HAP (JCPDS: 00-009-0432), are shown in Fig. 1.

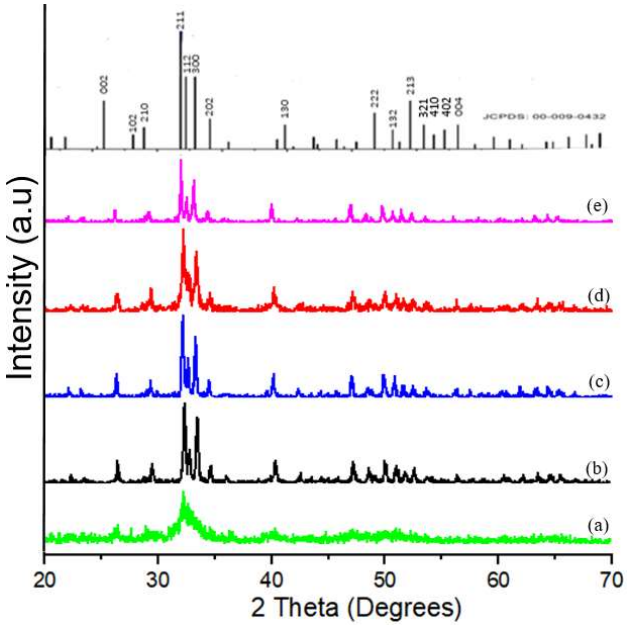

Figure 1: Diffractograms of CB samples compared with standard HAP - **(a)** uncalcined sample; **(b)** 50 μ, **(c)** 150 μ, **(d)** 250 μ and **(e)** 350 μ CB calcined samples.

Major crystallographic (hkl) planes for HAP (002), (210), (211), (112), (022), (310), (222) and (213) are identified in Fig. 1, where most intense is (211) plane. It can be

observed that the uncalcined sample displayed an amorphous phase with low intensity and a broader peak. This could be attributed to the significant presence of organic matter such as collagen in the uncalcined bone. However, amorphous phase disappeared at calcination temperature of 900 °C, indicating a complete removal of organic matter present in the bone matrix at this temperature. This conforms with the works of [33] and [2], which indicated that animal bone calcined at high temperatures (≥ 700 °C) displays intense and sharp peaks, proving crystallinity and complete removal of organic matter. It can also be observed from Fig. 1 and Table 1 that, as peaks shift to the left, lower Bragg's angle, or lower FWHM, evolved crystallite increases according to Eq. (2). It is assumed that reduction in FWHM triggers formation of HAP crystals, giving way to growth in crystallite sizes [34]. Shift in 2θ degree might be attributed to removal of OH radicals due to de-hydroxylation of HAP phase, which would cause a small degree of peak shifting in XRD finger prints [35]. Fig. 1 also shows the presence of identical phases in calcined samples that are similar to phases found in standard HAP [2], proving evolution of HAP. It is noteworthy that intensities varied among calcined samples with different SPS, and declined with a decrease in SPS.

Degree of crystallinity and evolved crystallite size

It can be observed from Table 1 and Fig. 2 that SPS of the bone material has a direct relationship with the degree of crystallinity and evolved crystallite size.

Table 1: Degree of crystallinity, FWHM and crystallite size of CB samples calcined at 900 °C/3 h.

SPS of CB samples (μm)	**Degree of crystallinity (%)**	**FWHM (°)**	**Crystallite size D (nm)**
50	66.9	0.283	31
150	85.8	0.220	42
250	86.0	0.189	51
350	88.6	0.177	56
Control/uncalcined CB	diffuse	-	-

Degree of crystallinity and evolved crystallite size increased with larger SPS. It is also noted that SPS of the bone material, degree of crystallinity and evolved crystallite size have an inverse relationship with FWHM. Inverse relationship between FWHM and degree of crystallinity has been observed by [36, 37]. The sample with greatest SPS (350 μm) had highest degree of crystallinity (88.6%), while the one with smallest SPS (50 μm) had lowest degree of crystallinity (66.9%). It is noteworthy from this work that SPS of the bone material influences crystallite size of evolved HAP and its crystallinity, which suggests that obtaining small-grained HAP by calcination requires small SPS of bone material [6, 38].

It has been equally recognized that degree of crystallinity varies with evolved crystallite size, both increasing with an increase in temperature [1]. In this work, a large SPS of bone material favours emergence of bigger crystallites with high crystallinity. In its turn, small SPS of bone material leads to the formation of smaller-sized HAP that is less crystalline. Crystallite size increases with respect to temperature due to the tendency of particles to crystallize and agglomerate at high temperatures [35]. Hence, as evolved HAP sample becomes crystalline, crystal size increases. It has been observed that, as a HAP sample becomes crystalline, crystal size increases [39]. Since calcination was done at a constant temperature and holding time, degree of crystallization and agglomeration is assumed to be controlled by SPS of the bone material. Large SPS will crystallize into big grains, while small SPS will crystallize into reduced grains.

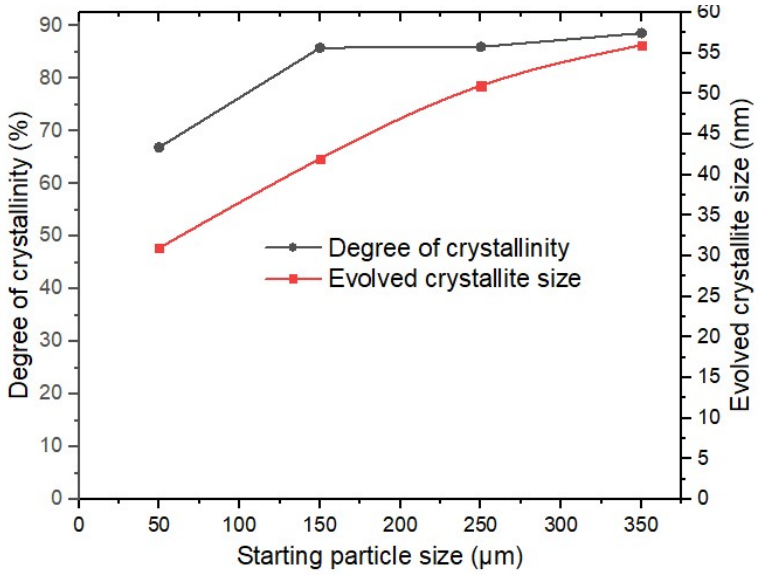

Figure 2: SPS *vs.* degree of crystallinity and evolved crystallite size of calcined CB waste.

Both degree of crystallinity and crystallite size are important properties of evolved HAP in medical applications, and both vary with SPS of the bone waste material. While crystallite size of HAP affects its bioactivity, biocompatibility and drug release [40], degree of crystallinity also affects drug's loading capacity, release rate [27] and bioresorption [28]. According to [27], while higher crystallinity could slow down drug release rate, lower crystallinity could enhance its loading capacity. It has been equally reported by [28] that high-crystalline HAP has very low or no activity towards bio-resorption, which is an important requirement for formation of chemical bonding with surrounding hard tissues. Crystalline HAP is more soluble in physiological environments and more metabolically active than a fully developed crystalline HAP

structure. Therefore, maneuvering crystallite size, degree of crystallinity and other properties of evolved HAP will remain at the forefront of HAP production.

Elemental composition and Ca/P ratios of uncalcined and calcined samples

Elemental composition obtained by EDX analysis of uncalcined and calcined CB samples with different SPS is shown in Fig. 3 and Table 2.

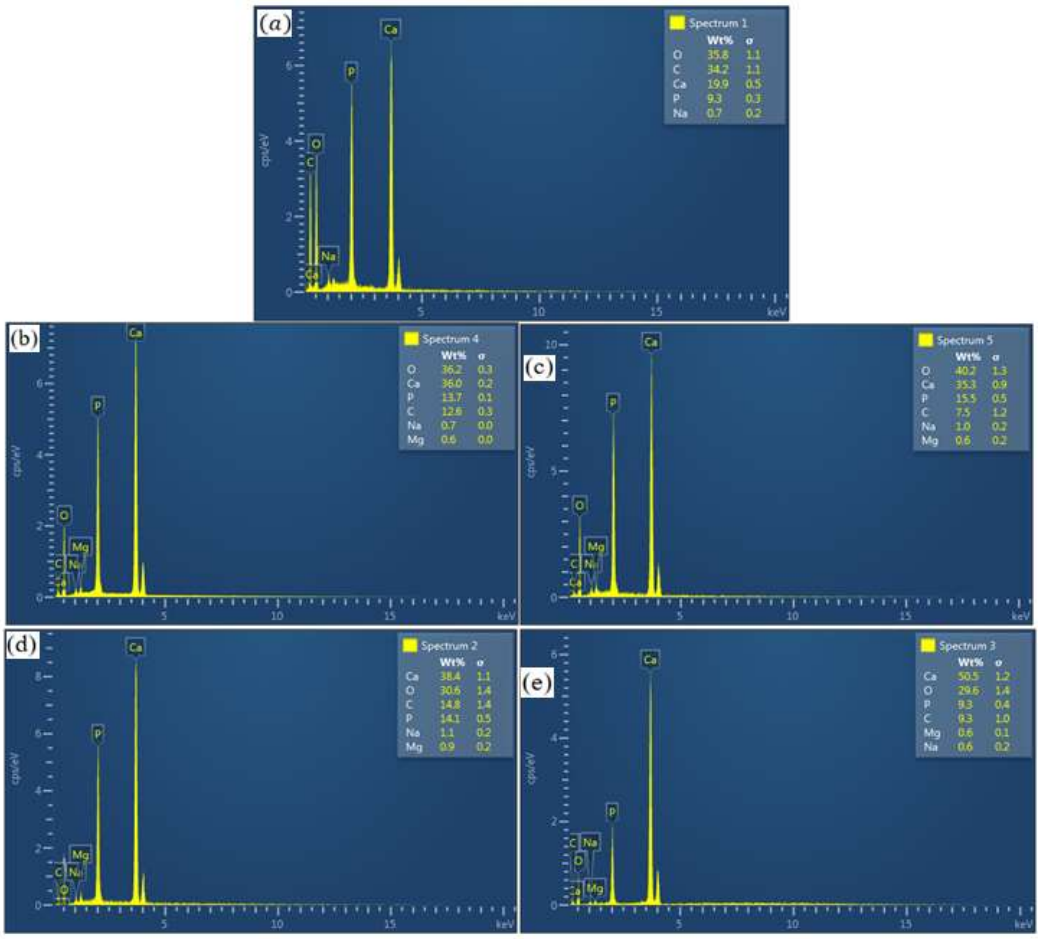

Figure 3: EDS results- **(a)** uncalcined sample, **(b)** 50 µ, **(c)** 150 µ, **(d)** 250 µ and **(e)** 350 µ CB calcined samples.

Table 2: Elemental composition and Ca/P ratio of uncalcined and samples calcined at 900 °C/3h.

SPS of CB samples (µm)	Elemental composition (wt.%)						
	Ca	P	O	C	Na	Mg	Ca/P ratio
50	36.0	13.7	36.2	12.6	0.7	0.6	2.28
150	35.3	15.5	40.2	7.5	1.0	0.6	2.63
250	38.4	14.1	30.6	14.8	1.1	0.9	2.72
350	50.5	9.9	29.6	9.3	0.6	0.6	5.43
Uncalcined CB	19.9	9.3	35.8	34.2	0.7	-	2.14

Table 2 shows significant presence of Ca, O, P and C in both uncalcined and calcined bone samples. Only two trace elements, Na and Mg, were detected in crystal lattice. C and O abound in raw samples, which is not unexpected, as they are main constituents of collagen (a protein), a significant organic matter in bones. O and C contents, which were 35.8 and 34.2 wt. % in the raw sample, decreased to 29.6 and 9.3% in 350 μm SPS sample, respectively. This might be attributed to the fact that calcination process expels organic substances from animal bones and as such, elements associated with organic matter will be reduced in the crystal lattice of the samples after calcination [2, 41], leaving behind mineral phase of bone (HAP). However, this reduction in O and C appears to be dependent on SPS, as it is the major parameter, because calcination was carried out at a fixed temperature and holding time. Reduction in O and C could be attributed to the fact that finer particles generally lead to faster reaction rates, and these cause more complete combustion and decomposition of the organic matrix and diffusion of gaseous products such as CO_2 out of CB material during calcination [42]. SPS has been shown to have a meaningful impact on C and O isotope composition of bone HAP [43].

Ca and P in raw samples increased from 19.9to 50.5% and 9.3 to 9.9% in 350 μm SPS sample. Both increases follow decrease in C and O at a calcination temperature of 900 °C, and are SPS dependent, though not directly proportional to its increase. The observed trend of increased Ca and P levels in calcined samples aligned with a decrease in C and O contents. This phenomenon is attributed to the higher surface areas of smaller grain sizes, facilitating efficient reactions and escape of organic matter. Consequently, this process results in higher concentrations of Ca and P.

Calculated Ca/P ratios of both uncalcined and calcined CB samples calcined at 900 °C, for 3 h, with varying SPS, are also presented in Table 2 and plotted in Fig. 4.

Ca/P ratios deviate from theoretical value of 1.67 for pure stoichiometric HAP [2]. However, it has been noted that natural HAP exhibits a Ca/P ratio higher than 1.67 [44, 45].

Ca/P ratio of calcined samples is higher than as-received CB, and fluctuates between 2.28 and 5.43, increasing with larger SPS. Since Ca/P ratio decreases with reduced SPS, it is expected that processing (grinding and sieving) to obtain small SPS will lead to a Ca/P ratio closer to that of standard HAP. High Ca/P ratio (5.43) exhibited by 350 μ starting bone material, as shown in Table 2 and Fig. 4, could not be explained at this stage. However, many factors have been identified that could lead to a fluctuation of Ca/P ratio from theoretical value, which include calcination conditions such as holding temperature, time and atmosphere of calcination process; presence of ions such as Ca^{2+}, PO_4^{3-} and OH^- in natural bone tissues; and their intensity, which may vary depending on the nutrition and diet of the source animal [45].

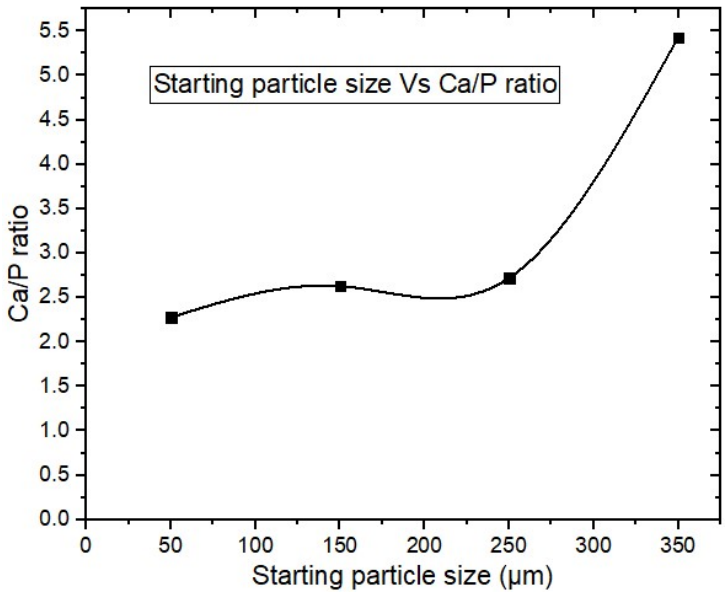

Figure 4: SPS *vs*. Ca/P ratio of calcined CB waste.

SEM analysis of uncalcined and calcined CB powder samples

Images of uncalcined and calcined CB powders obtained with SEM are shown in Fig. 5.

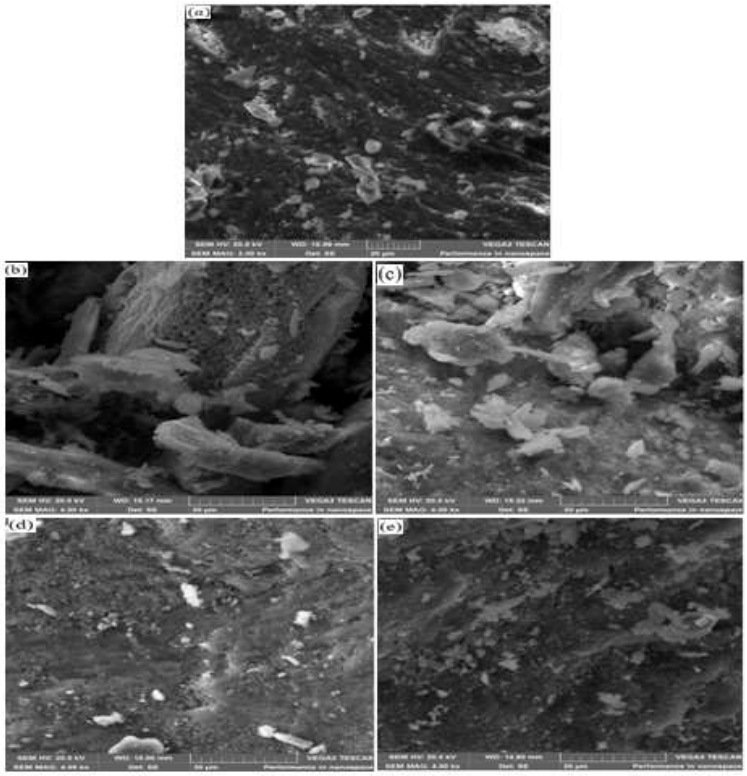

Figure 5: Morphology of calcined CB powders- **(a)** uncalcined sample, **(b**) 50 μ, **(c)** 150 μ, **(d)** = 250 μ and **(e)** 350 μ CB samples.

Microstructures of the uncalcined sample (Fig. 5a) appear to be dark and dense due to the presence of organic material in CB matrix. Morphologies of calcined samples varied with an increase in SPS, forming a porous network that decreased with larger SPS. The bone material having smallest SPS (50 μm) appears to have most porous and agglomerated structure. Morphology of bone material having SPS of 150 μm (Fig. 5b) is irregular with enlarged pores, which could be ascribed to pore coalescence due to fast volatile release during calcination. 150 μ CB contained highest amount of O and lowest amount of C after calcination, suggesting incomplete decomposition of organic material therein, which leads to the formation of enlarged voids and leaves behind a grey microstructure [46].

It could be observed that porosity decreased and the structure became finer with an increase in SPS (Figs. 5 (c)–(e)). High porosity of 50 μ SPS bone material could be attributed to the reactivity of its small size caused by its large surface area, leading to easier removal of organic matter which left behind pores in the bone matrix after calcination at 900 °C. Thus, pores were reduced in samples with bigger SPS (Figs. 5 (c)–(e)), due to their lower reactivity.

Fourier transform infra-red spectroscopy

FTIR spectra of the uncalcined sample and samples having different SPS and calcined at 900 °C, for 3 h, are shown in Fig. 6.

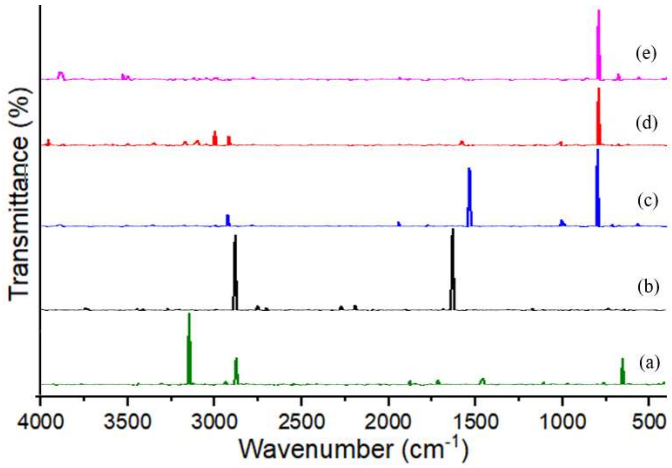

Figure 6: FTIR of - **(a)** uncalcined sample, **(b**) 50 μ, **(c)** 150 μ, **(d)** = 250 μ and **(e)** 350 μ CB samples.

Sharp peak at 3143.3 cm^{-1} is indicative of a lower concentration of OH^- group in uncalcined sample. A strong presence of CO_3^{2} group in uncalcined sample is seen at 2870.5, 1865.1, 1711.6, 1453.1 and 796.4 cm^{-1}, while that of PO_4^{3-} group is at 1027.6

and 642.9 $cm^{-1.}$ The band at frequency numbers from 1628 to 1412 cm^{-1} has been ascribed to asymmetric stretching vibration for CO_3^2 [6].
Calcination at a temperature of 900 °C for 3 h made OH^- bands in calcined samples broader, signifying a greater presence of OH^- group. Increase in concentration of OH^- group may be attributed to hydroxylation process that introduces OH^- functional group into crystal structure of evolved HAP [47], and is dependent on SPS of the bone material. Increase in concentration (decrease in transmittance) of OH^- group can be attributed to removal of organic material (C-O-bearing components) because of high-temperature treatment [47].
CO_3^2 and PO_4^{3-} groups identified in uncalcined samples also decreased in concentration after calcination at 900 °C for 3 h. Robust absorption bands (low transmittance) identified at approximately 1027.6 and 642.9 cm^{-1} in calcined samples correspond to stretching vibrations of PO_4^{3-} in HAP, affirming the strong presence of PO_4^{3-} groups in calcined bone sample. PO_4^{3-} group is more concentrated in calcined samples than in uncalcined ones, which supports observed increase in P content in EDX result of calcined samples with larger SPS. Reduction in concentration of CO_3^2 group equally supports observed decrease in C content in EDX result of calcined sample with an increase in SPS.

Conclusion

This work sought to establish whether SPS is an important processing parameter on evolution of HAP from CB waste powder subjected to calcination, by considering its effect on physico-chemical properties of evolved HAP. Physico-chemical properties considered included degree of crystallinity, evolved crystallite size, C-to-P ratio, concentration of essential elements and functional groups, all of which determine suitability of HAP for biomedical applications. CB waste material was processed to obtain particles of 50, 150, 250 and 350 μm, which were heated to a constant temperature and holding time of 900 °C, for 3 h, to enable their transformation into HAP. Evolved HAP was characterized to determine physico-chemical properties.
XRD results revealed diffraction patterns that were characteristic peaks of HAP. Degree of crystallinity of HAP increased with greater SPS, and bone material, having highest SPS (350 μm), was the most crystalline. Evolved crystallite sizes were also sensitive to SPS, increasing with larger SPS and decreasing with smaller on. This suggests that both crystallinity and evolved crystallite size of HAP could be manoeuvered with SPS of the bone material. Evolved crystallite size and crystallinity are essential physical properties of HAP that affect its drug's loading capacity, release rate and bio-resorption.
Based on EDX results, essential elements in HAP, such as Ca, P, O and C, also varied according to particle size, with Ca increasing with larger SPS. P, O and C decreased with an increase in SPS. Variation in concentration of essential elements affects Ca/P

ratio, another important quality of HAP intended for biomedical application. Although Ca/P ratio of calcined samples deviated from theoretical value of 1.67 for pure stoichiometric HAP, it decreased with reduced SPS. This suggests that processing (grinding and sieving) to obtain SPS could lead to a Ca/P ratio closer to that of standard HAP.

FTIR spectra indicated the presence of characteristic vibrational bands of OH-, PO_4^{3-}, and CO_3^{2-} groups associated with HAP. However, concentration of functional groups is sensitive to SPS, with concentrations of OH- and PO_4^{3-} groups increasing, while those of CO_3^{2-} group decreased with larger SPS of bone waste material.

This work has clearly demonstrated that SPS is an important processing parameter that affects physico-chemical properties of HAP extracted from CB waste, such as temperature and holding time. However, further work is required to optimize effects of SPS, temperature and holding time, to yield the best combination of these properties for biomedical applications.

Acknowledgements

The authors would like to acknowledge the Nano Research Laboratory, University of Nigeria, Nsukka, for assistance in XRD and FTIR analysis, and the Department of Mechanical Engineering Science, University of Johannesburg, Auckland Park, South Africa, for assistance in conducting SEM and EDX analysis.

Authors' contributions

Obayi C. S: Conceived and designed the analysis; wrote the paper. **Ugwu E. C.**: collected data; inserted data; wrote the paper. **Ekedebe P. C.**: performed the analysis; **Obe H. A.**: performed the analysis. **Egbuhuzor M. O**: inserted data or analysis tools; performed the analysis. **Offor P. O.**: inserted data or analysis tools; performed the analysis. **Nnamchi P. S.**: funded the project from his grant.

Abbreviations

CB: cattle bone
CO_3^{2-}: carbonate
EDX: Energy dispersive X-ray spectroscopy
FTIR: Fourier transform infrared spectroscopy
FWHM: full width at half maximum of the peak
HAP: Hydroxyapatite
OH^-: Hydroxyl
PO_4^{3-}: Phosphate
SEM: Scanning electron microscopy
SPS: starting particle size
XRD: X-ray diffraction

References

1. Anita LJ, Ravichandran K and Sundareswari M. The study on the synthetic methodologies for manoeuvring the morphology crystallinity and particle size of hydroxyapatite. J Chem Pharm Res. 2015;7(2):231-39.
2. Olusola EO, Olatunde IS, Ilomuanya MO et al. Structural and morphological evaluations of natural hydroxyapatite from calcined animal bones for biomedical applications. J Cast Mater Eng. 2022;6(1):14-2. https://doi.org/10.7494/jcme.2022.6.1.14
3. Ismail SA, Abdullah HZ. Extraction and characterization of natural hydroxyapatite from goat bone for biomedical applications. Mater Sci For. 2020;1010:573-78. https://doi.org/10.4028/www.scientific.net/MSF.1010.573
4. Yazdi AFA, Yazdani A, Khozani TT et al. Extraction and viability checking of various carbonated hydroxyapatite by Wharton's jelly mesenchymal stem cell. Sci Int. 2013;1(5):132-38. https://doi.org/10.5567/sciintl.2013.132.138
5. Akram M, Ahmed R, Shakir I et al. Extracting hydroxyapatite and its precursors from natural resources. J Mater Sci. 2014;49:1461-75. https://dx.doi.org/10.1007/s10853-013-7864-x
6. Khoo W, Nor FM, Ardhyananta H et al. Preparation of natural hydroxyapatite from bovine femur bones using calcination at various temperatures. Proced Manuf. 2015;2:196-201. https://doi.org/10.1016/j.promfg.2015.07.034
7. Bahrololoom ME, Javidi M, Javadpour S et al. Characterization of natural hydroxyapatite extracted from bovine cortical bone ash. J Ceram Proc Res. 2009;10 (2):129-38.
8. Mondal B, Mondal S, Mondal A et al. Fish scale derived hydroxyapatite scaffold for bone tissue engineering. Mater Char. 2016;121:112-24. http://dx.doi.org/10.1016/j.matchar.2016.09.034
9. Fara ANK, Abdullah HZ. Characterization of natural hydroxyapatite (HAP) derived from different types of tilapia fish bones and scales. Malays J Microsc. 2014;10:34-40. https://doi.org/10.1063/1.4919215
10. Kumar CS, Dhanaraj K, Vimalathithan RM et al. Hydroxyapatite for bone related applications derived from sea shell waste by simple precipitation method. J Asian Ceram Soc. 2020;8(2):416-29. https://doi.org/10.1080/21870764.2020.1749373
11. El-Bassyouni GT, Eldera SS, Kenawy SH et al. Hydroxyapatite nanoparticles derived from mussel shells for in vitro cytoxicity test and cell viability. Heliyon. 2020;6:e04085. https://doi.org/10.1016/j.heliyon.2020.e04085
12. Fahami A, Ebrahimi-Kahrizsangi R, Nasiri-Tabrizi B. Mechanochemical synthesis of hydroxyapatite/titanium nanocomposite. Solid State Sci. 2011;13(1):135-41. https://doi.org/10.1016/j.solidstatesciences.2010.10.026

13. Rhee SH. Synthesis of hydroxyapatite via mechanochemical treatment. Biomatter. 2002;23(4):1147-52. https://doi.org/10.1016/S0142-9612(01)00229-0
14. Mohd PNAS, Alipal J, Abdullah HZ et al. Synthesis of eggshell derived hydroxyapatite via chemical precipitation and calcination method. Mater Tod: Proceed. 2021;42(1):172-77. https://doi.org/10.1016/j.matpr.2020.11.276
15. Hassan MN, Mahmoud MM, Link G et al. Sintering of naturally derived hydroxyapatite using high frequency microwave processing. J Alloys Compd. 2016;682:107-14. https://doi.org/10.1016/j.jallcom.2016.04.266
16. Pramanik S, Agarwal AK, Rai KN et al. Development of high strength hydroxyapatite by solid-state-sintering process. Ceram Int. 2007;33(3):419-26. https://doi.org/10.1016/j.ceramint.2005.10.025.
17. Yelten-Yilmaz A, Yilmaz S. Wet chemical precipitation synthesis of hydroxyapatite (HA) powders. Ceram Int. 2018;44(8):9703-10. https://doi.org/10.1016/j.ceramint.2018.02.201
18. Piccirillo C, Pullar RC, Costa E et al. Hydroxyapatite-based materials of marine origin: A bioactivity and sintering study. Mater Sci Eng C. 2015;51:309-15. https://doi.org/10.1016/j.msec.2015.03.020
19. Ramirez-Gutierrez CF, Londoño-Restrepo SM, del Real A et al. Effect of the temperature and sintering time on the thermal, structural, morphological and vibrational properties of hydroxyapatite derived from pig bone. Ceram Int. 2017;43:7552-59. https://doi.org/10.1016/j.ceramint.2017.03.046
20. Akhlis RSN, Bayuseno AP, Ismail R et al. Review of the temperature and holding time effects on hydroxyapatite fabrication from the natural sources. J Biomed Sci Bioeng. 2021;1(1):27-31. https://doi.org/10.14710/jbiomes.2021.v1i1.27-31
21. Prokopiev O, Sevostianov I. Dependence of the mechanical properties of sintered hydroxyapatite on the sintering temperature. Mater Sci Eng A. 2006;431(1-2):218-27. https://doi.org/10.1016/j.msea.2006.05.158
22. Sudeep P, Anindya P, Amit RC et al. Effect of trace elements on the sintering effect of fish scale derived hydroxyapatite and its bioactivity. Ceram Int. 2017;43(17):15678-84. https://doi.org/10.1016/j.ceramint.2017.08.127
23. Fihri A, Len C, Varma RS et al. Hydroxyapatite: A review of syntheses, structure and applications in heterogeneous catalysis. Coord Chem Rev. 2017;347:48-76. https://doi.org/10.1016/j.ceramint.2017.08.127
24. Ramirez-Gutierrez CF, Londoño-Restrepo SM, del Real A et al. Effect of the temperature and sintering time on the thermal, structural, morphological and vibrational properties of hydroxyapatite derived from pig bone. Ceram Int. 2017;43:7552-59. https://doi.org/10.1016/j.ceramint.2017.03.046

25. Ramesh S, Natasha AN, Tan CY et al. Direct conversion of eggshell to hydroxyapatite ceramic by a sintering method. Ceram Int. 2016;42:7824-29. https://doi.org/10.1016/j.ceramint.2016.02.015
26. Ghedjemis A, Ayeche R, Benouadah A. A comparative study on properties of hydroxyapatite prepared from bovine and dromedary bone. J Aust Ceram Soc. 2022;58:607-16. https://doi.org/10.21203/rs.3.rs-794688/v1
27. Zhang H, Yan D, Gedara SMK et al. View effects of crystallinity and surface modification of calcium phosphate nanoparticles on the loading and release of tetracycline hydro-chloride. IOP Conf Series: Mater Sci Eng. 2017;182:012052. https://doi.org/10.1088/1757-899X/182/1/012052
28. Sanosh KP, Chu M-C, Balakrishnan A et al. Preparation and characterization of nano-hydroxyapatite powder using sol-gel technique. Bull Mater Sci. 2009;32(5):465-47. https://doi.org/10.1007/s12034-009-0069-x
29. Zhou H, Lee J. Nanoscale hydroxyapatite particles for bone tissue engineering. Acta Biomat. 2011;7:2769-81. https://doi.org/10.1016/j.actbio.2011.03.019
30. Wang J, Shaw LL. Nanocrystalline hydroxyapatite with simultaneous enhancements in hardness and toughness. Biomaterials. 2009;30(34):6565-72. https://doi.org/10.1016/j.biomaterials.2009.08.048
31. Odusote JK, Danyuo Y, Baruwa AD et al. Synthesis and characterization of hydroxyapatite from bovine bone for production of dental implants. J Appl Biomat Funct Mat. 2019;17(2):1-7. https://doi.org/10.1177/2280800019836829
32. Rana M, Akhtar N, Rahman S et al. Extraction of hydroxyapatite from bovine and human cortical bone by thermal decomposition and effect of gamma radiation: A comparative study. Int J Complement Alt Med. 2017;8(3):00263. https://doi.org/10.15406/ijcam.2017.08.00263
33. Blanco A, Monte MC, Campano C et al. Nanocellulose for industrial use: cellulose nanofibers (CNF), cellulose nanocrystals (CNC) and bacterial cellulose (BC). In: C.M. Hussain, Handbook of Nanomaterials for Industrial Applications. Elsevier. 2018:74-126.
34. Restrepo RV, Arellano-Ramírez ID, Alzate-Acevedo N et al. Influence of the calcination temperature on the crystallographic, compositional and morphological properties of natural hydroxyapatite obtained from sheep bones. Sci Tech. 2021;26(4):525-31. https://doi.org/10.22517/23447214.24888
35. Jojor LM, Bambang S, Decky JI. Characterization of Hydroxyapatite Derived from Bovine Bone. Asian J Appl Sci. 2015;3(4):758-65.
36. Ghedjemis A, Ayeche R, Benouadah A. A comparative study on physicochemical properties of hydroxyapatite powder prepared from bovine and dromedary bone. J Aust Ceram Soc. 2022;58:607-16. https://doi.org/10.1007/s41779-022-00721-6

37. O-Restrepo SL, Ramirez-Gutierrez CF, del Real A et al. Study of bovine hydroxyapatite obtained by calcination at low heating rates and cooled in furnace air. J Mater Sci. 2016;51:4431-41. https://doi.org/10.1007/s10853-016-9755-4
38. Hossain MS, Mahmud M, Sultana S et al. Coupled effect of particle size of the source materials and calcination temperature on the direct synthesis of hydroxyapatite. R Soc Open Sci. 2021;8:210684. https://doi.org/10.1098/rsos.210684.
39. Poralan GM Jr, Gambe JE, Alcantara EM et al. X-ray diffraction and infrared spectroscopy analyses on the crystallinity of engineered biological hydroxyapatite for medical application, IOP Conf Series: Mater Sci Eng. 2015;79:012028. https://doi.org/10.1088/1757-899X/79/1/012028
40. Sasikumar S. Effect of particle size of calcium phosphate based bioceramic drug delivery carrier on the release kinetics of ciprooxacin hydrochloride: An in-vitro study. Front Mater Sci Chin. 2013;7(3):261-68. https://doi.org/10.1007/s11706-013-0216-6
41. Ofudje EA, Rajendran A, Adeogun AI et al. Synthesis of organic derived hydroxyapatite scaffold from pig bone waste for tissue engineering applications. Adv Powd Technol. 2017;29(1):1-8. https://doi.org/10.1016/j.apt.2017.09.008
42. Alaoui NS, Laghdach AE, Correa EMC et al. Preparation of bone chars by calcination in traditional furnace. J Mater Environ Sci. 2014;5(2):476-83.
43. Moloughney VP, Pinder DM, Pestle WJ. Particle size matters: The effect of particle size on carbon and oxygen isotope composition of bone hydroxyapatite. Am J Phys Anthropol. 2020;171(4):718-24. https://doi.org/10.1002/ajpa.24006
44. Figueiredo M, Fernando A, Martins G et al. Effect of the calcination temperature on the composition and microstructure of hydroxyapatite derived from human and animal bone. Ceram Int. 2010;36(8):2383-93. https://doi.org/10.1016/j.ceramint.2010.07.016
45. Sofronia AM, Baies R, Anghel EM et al. Thermal and structural characterization of synthetic and natural nanocrystalline hydroxyapatite. Mater Sci Eng: C. 2014;43:153-63. https://doi.org/10.1016/j.msec.2014.07.023
46. Öksüz KE, Kilinç S, Öze A. Effect of Calcination on Microstructure development and properties of hydroxyapatite powders extracted from human and bovine bones. Trans Ind Ceram Soc. 2019;78(1):41-45. https://doi.org/10.1080/0371750X.2019.1588170
47. Ooi C, Hamdi M, Ramesh S. Properties of hydroxyapatite produced by annealing of bovine bone. Ceram Int. 2007;33:1171-77. https://doi.org/10.1016/j.ceramint.2006.04.001